

Accepted Manuscript

Research paper

Structural and spectroscopic investigations of redox active seven coordinate luminescent lanthanide complexes

Jennifer K. Molloy, Lionel Fedele, Olivier Jarjayes, Christian Philouze, Daniel Imbert, Fabrice Thomas

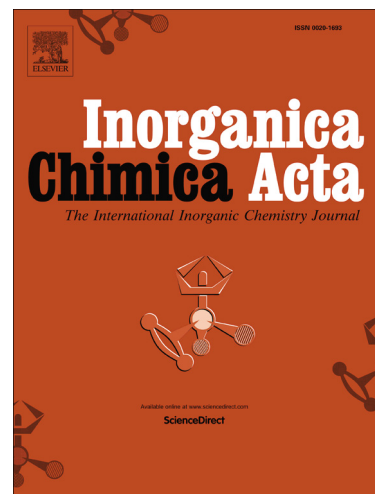
PII: S0020-1693(18)31184-8
DOI: <https://doi.org/10.1016/j.ica.2018.08.054>
Reference: ICA 18454

To appear in: *Inorganica Chimica Acta*

Received Date: 28 July 2018
Accepted Date: 30 August 2018

Please cite this article as: J.K. Molloy, L. Fedele, O. Jarjayes, C. Philouze, D. Imbert, F. Thomas, Structural and spectroscopic investigations of redox active seven coordinate luminescent lanthanide complexes, *Inorganica Chimica Acta* (2018), doi: <https://doi.org/10.1016/j.ica.2018.08.054>

This is a PDF file of an unedited manuscript that has been accepted for publication. As a service to our customers we are providing this early version of the manuscript. The manuscript will undergo copyediting, typesetting, and review of the resulting proof before it is published in its final form. Please note that during the production process errors may be discovered which could affect the content, and all legal disclaimers that apply to the journal pertain.



Structural and spectroscopic investigations of redox
active seven coordinate luminescent lanthanide
complexes

Jennifer K. Molloy,^{a*} Lionel Fedele,^{a,b} Olivier Jarjayes,^a Christian Philouze,^a Daniel Imbert,^b
Fabrice Thomas^{a*}

^a Département de Chimie Moléculaire, Univ. Grenoble Alpes, UMR-5250 CNRS UGA, CS 40700, 38058 Grenoble Cedex 9, France. Email : jennifer.molloy@univ-grenoble-alpes.fr; fabrice.thomas@univ-grenoble-alpes.fr. <http://dcm.univ-grenoble-alpes.fr/CIRE>

^b Univ. Grenoble Alpes, CNRS, CEA, INAC-SyMMES, 38000 Grenoble, France.

Abstract

The ligand H_3L and its corresponding tris(phenolato) lanthanide complexes **L-Tb**, **L-Gd**, **L-Yb** and **L-Lu** were synthesized. The X-Ray crystal structures demonstrated a monocapped octahedron environment of the lanthanide ion, with exclusion of all solvent molecules from the coordination sphere due to the protection by the *tert*-butyl groups. The coordination bond distances followed the lanthanide contraction, with Ln-O bond lengths in the range 2.148-2.217 Å and Ln-N_{imine} bond lengths in the range 2.405-2.535 Å. Each of the complexes showed three one-electron oxidation processes. These potentials changed as a function of the lanthanide due to the difference in size of the metal ions. Both chemical and electrochemical oxidation of these complexes permitted the one-electron oxidised species to be generated. They all show a sharp absorption band at around 420 nm in their UV-Vis spectra, which demonstrated phenoxyl radical formation. Consistently, the radical species **L-Lu**⁺ displays a resonance at $g = 2.001$ in its EPR spectrum. The other cations are EPR-silent or difficult to detect due to magnetic interactions, confirming the proximity of the phenoxyl radical to the metal centre. For both **L-Lu**⁺ and **L-Yb**⁺ DFT calculations predict the radical to be delocalized over the three arms. The **L-Tb** and **L-Yb** complexes experienced a quenching of the luminescence upon oxidation to the radical species whereby the quenching of up to 83 % in the visible region and 93 % in the NIR was observed.

Keywords

Phenoxyl; Radical; Redox Noninnocent ligand; Lanthanides; Luminescence.

1. Introduction

Medical imaging has become a significantly important subject with increasing need for more specific and selective imaging techniques. [1, 2] Changes in redox activity within cells and tissues are associated with some of the most lethal pathologies of the 21st century, including cardiac and neurodegenerative diseases, as well as cancers.[3-9] A non-invasive detection and imaging of hypoxic regions in tissues could for example allow the more efficient and selective detection of tumors. [7, 10-13] The use of lanthanide complexes can permit very selective and easy to detect signals. [14-16] However, lanthanide ions cannot inherently be used as detectors of redox or hypoxic environments due to their propensity to remain in their (+III) oxidation state. The use of a redox sensitive ligand could circumvent these problems and confer redox activity on the complex. Very few examples of lanthanide complexes have been reported with a redox stimulus or reaction with reactive oxygen species resulting in a change in properties of the complex. [17-27] We have recently demonstrated the use of redox active lanthanide complexes whereby a redox stimuli resulted in a quenching of the lanthanide luminescence. [27, 28] The tripodal ligands were based on para-methoxy substituted phenolates (Chart 1) whereby the phenolates demonstrate oxidation which affects the luminescence of the complexes.[27] We observed an interesting trend in oxidation potentials for a series of complexes ($L_n = \text{Nd, Eu, Gd, Tb, Er, Yb, Lu}$), whereby the larger lanthanide complexes show the smaller values, with a decreased $\Delta E_{1/2}$ between each consecutive wave. The methoxy group exerts an electron-donating effect that is necessary for stabilizing phenoxy radical species. However it usually results in small $\Delta E_{1/2}$, i.e. a poor separation of the consecutive redox processes,[29-36] which may be detrimental for selectivity and quantification. The corresponding para *tert*-butyl derivatives could confer a better separation of oxidation potentials, as demonstrated in several d-transition metal complexes,[29, 34, 37] while still stabilizing satisfactorily phenoxy radicals.[38] Herein we present a series of lanthanide(III) complexes ($L_n = \text{Gd, Tb, Yb, Lu}$) based on the ligand H_3L (Chart 1),[39, 40] which harbours three redox-active di-*tert*-butyl-phenol moieties. We investigated the spectro-electrochemical properties (voltammetry, UV-vis, EPR) of the complexes and establish that the redox activity can be conferred by the redox active ligand coordinated to the metal ions. For the Tb(III) and Yb(III) complexes, which feature a visible- and NIR-emitter, respectively, we demonstrated that a change in oxidation state of the ligand induces a strong quenching of the luminescence (83 % and 93 %, respectively).

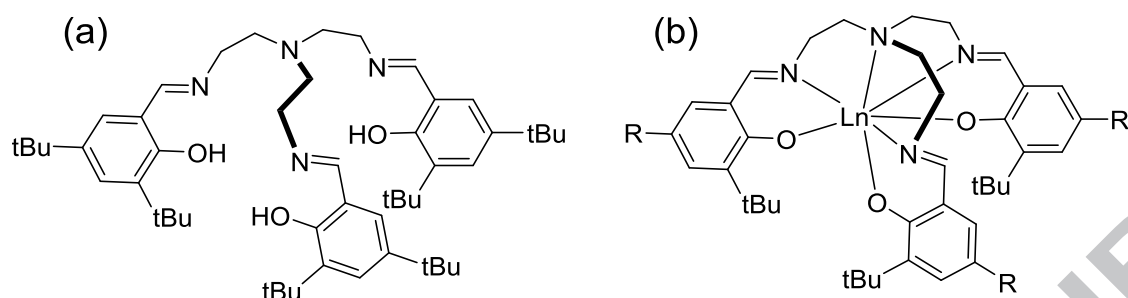


Chart 1. Structures of (a) the ligand H_3L and (b) the lanthanide complexes $L-Ln$ ($R = t-Bu$) and $L^{OMe}-Ln$ ($R = OMe$)

2. Experimental

2.1 Materials and methods

All chemicals were of reagent grade and were used without purification. NMR spectra were recorded on a Bruker AM 300 (1H at 300 MHz) spectrometer. Chemical shifts are quoted relative to tetramethylsilane (TMS). Mass spectra were recorded on an ESI/QTOF Waters Xevo G2-S apparatus. The FTIR spectra were recorded using a Nicolet iS10 spectrometer on crystalline material (ATR mode). UV/Vis spectra were recorded on a Cary Varian 50 spectrophotometer equipped with a Hellma immersion probe (1.000 cm path length). The temperature in the cell was controlled using a Lauda circulating bath. Luminescence data were recorded both at room and low temperature using a modular Fluorolog FL3-22 spectrometer from Horiba-Jobin Yvon-Spex equipped with a double grating excitation monochromator and an iHR320 imaging spectrometer. Hamamatsu R928P and R5509 photomultipliers were used for visible and NIR measurements, respectively. All spectra were corrected for detection and optical spectral response (instrumental functions) of the spectrofluorimeters. X-band EPR spectra were recorded on a Bruker EMX Plus spectrometer equipped with a Bruker Helium flow cryostat and a dual mode cavity. Stopped Flow experiments were performed on a Bio-Logic SFM 20 apparatus, connected to a Tidas J&M diode array spectrometer and using a Hamamatsu UV-Vis source. The temperature was set at 233 K by using a Haake Phoenix II immersion bath. Electrochemical measurements were carried out using a CHI 620 potentiostat. Experiments were performed in a standard three-electrode cell under argon atmosphere. A glassy carbon disc electrode (3 mm diameter), which was polished with 1 mm diamond paste, was used as the working electrode. The

auxiliary electrode is a platinum wire, while the reference was an Ag/AgNO₃ 0.01 M in CH₃CN. All the potentials are given vs. the Fc⁺/Fc redox couple, which was used as standard.

2.2 Synthesis

L-Tb. The ligand H₃L (0.050 g, 0.063 mmol, 1 eq.) [39, 40] was dissolved in MeOH (5 mL) and heated to 60 °C. The salt Tb(NO₃)₃·6H₂O (0.032 g, 0.064 mmol, 1 eq.) was added and stirred at 60 °C for 5 minutes. After 5 minutes Et₃N (26 μL, 0.190 mmol, 3 eq.) was added to the solution. The complex was stirred for 30 minutes and then cooled to room temperature and filtered on a sintered glass funnel. The solid was redissolved in CH₃CN/CH₂Cl₂ whereby slow evaporation of the solvent afforded green single crystals of **1-Tb**. Yield: 0.035 g (54 %). HR-ESIMS: m/z observed 951.5189 for C₅₁H₇₅N₄O₃Tb, calcd, 951.5171 [M+H]⁺. Elemental Analysis calculated for C₅₄H₈₂Cl₂N₅O₄Tb (M + CH₂Cl₂ + CH₃CN + H₂O) C: 59.23 H: 7.55 N: 6.40 experimental 60.48 H: 7.60 N 6.24.

L-Yb. The complex was prepared in a similar manner than **L-Tb** to yield yellow crystals 0.025 g of **L-Yb**, yield 63 %. HR-MS (Q-TOF): **L-Yb**, m/z, 966.5313; Calcd: 966.5306 for [M+H]⁺. Elemental Analysis, Calculated C: 63.26 H: 7.81, N:6.96 for C₅₁H₇₅N₄O₃Yb (M+CH₃CN), experimental C 61.18 H: 7.77 N: 7.05.

L-Lu. The complex was prepared in a similar manner than **L-Tb**, isolated as yellow crystals 0.030 g of **L-Lu**, with a yield of 61 %. HR-ESIMS: m/z 967.5328; Calcd: 967.5325 for [M+H]⁺. ¹H NMR (CDCl₃, 400 MHz) 8.16 (s, 3H), 7.32 (3H, d, J = 2.4 Hz), 6.99 (3H, d, J = 2.4 Hz), 4.15 (3 H, t, J = 12.2 Hz, CH₂), 3.24 (3H, d, J = 12.2, CH₂), 2.88 (6H, m), 1.30 (27 H, CH₃, tBu), 0.98 (27 H, CH₃, tBu). ¹³C NMR (100 MHz, CDCl₃): 197.3, 167.9, 165.4, 139.6, 134.6, 128.6, 127.7, 120.9, 59.9, 57.6, 34.8, 33.8, 31.5, 31.3, 29.2. Elemental analysis; calculated for C₅₄H₈₀Cl₂LuN₅O₃ (M + CH₂Cl₂ + CH₃CN), C: 59.33 H: 7.38, N: 6.41, experimental C: 62.04, H: 7.53, N: 6.33.

L-Gd. The complex was prepared in a similar manner than **L-Tb**, isolated as yellow crystals, 0.043 g of **L-Gd**, with a yield of 73 %. HR-ESIMS: m/z **L-Gd**, m/z, 950.5133; Calcd: 950.5158 for [M+H]⁺. Elemental Analysis; calculated for C₅₁H₇₇GdN₄O₄ (+H₂O) C: 63.32 H: 8.02, N: 5.79, experimental C: 63.80 H: 8.20, N: 5.57.

2.3 X-Ray diffraction

Single crystals were coated with a mixture of parafins, picked up with nylon loops and mounted in the nitrogen cold stream of the diffractometer. Mo-K α radiation ($\lambda = 0.71073\text{\AA}$) from a Mo-target anode X-ray microfocus source equipped with INCOATEC Quazar Montel multilayer optic was used. Final cell constants were obtained from least squares fits of several thousand strong reflections. Intensity data were corrected for absorption using intensities of redundant reflections with the program SADABS. The structures were solved by charge flipping methods and subsequent difference Fourier techniques. The OLEX software was used for the refinement.[41] All non-hydrogen atoms were anisotropically refined and hydrogen atoms were placed at calculated positions and refined as riding atoms with isotropic displacement parameters. CCDC-1858222-1858225 contain the crystallographic data for **L-Ln** (Ln = Tb, Gd, Yb and Lu); these data can be obtained free of charge via <http://www.ccdc.cam.ac.uk/conts/retrieving.html>.

2.4 Computational details

The DFT calculations were performed by using the ORCA 3.01 package.[42] The geometry optimizations were performed with the B3LYP functional[43, 44] with the approximate relativistic scheme ZORA (zeroth order regular approximation)[45] and using the KDIIS and RIJCOSX algorithms.[46] The latter treats the Coulomb term via the split-RI-J method and the exchange term via seminumerical integration. Segmented all-electron relativistically contracted (SARC) basis sets[47] were used for the lanthanide ions, together with TZVP basis sets[48] for all the other atoms. Large grids (GridX7 in the Orca formalism) were used for the C,H,O,N atoms, with an even larger radial grid on the lanthanide ion (IntAcc = 20 in the Orca formalism).

3. Results and Discussion

3.1 Synthesis of the ligand and complexes

The tripodal ligand H₃L was synthesised in methanol by combining 3 eqs of 3,5-*ditert*-butyl-5-salicylaldehyde with 1 eq. of TREN.[39] The synthesis of the complexes **L-Gd**, **L-Tb**, **L-Yb** and **L-Lu** was performed using H₃L with a stoichiometric amount of the corresponding metal nitrate salt and a slight excess of triethylamine. The complexes were recrystallized by slow evaporation of a concentrated acetonitrile:dichloromethane solution. Single crystals suitable for X-Ray diffraction were obtained by this method. The single crystals were also utilised for all spectroscopic measurements. The vibrational spectra show that the C=N stretch of the ligand (1632 cm^{-1})[49] shifted to 1616 cm^{-1} for the lanthanide complexes as a result of

coordination of the imine. The ^1H NMR spectrum of **L-Lu** shows the imine resonance 8.16 ppm (singlet), as well as the distinctive resonances of the two H_{meta} of the salicylidene moieties at 7.32 and 6.99 ppm (doublets). The resonance of the *tert*-butyl groups are observed as two singlets at 1.30 and 0.98 ppm. This ^1H NMR spectrum supports a C_{3v} symmetry of the complex in solution, in agreement with that observed at the solid state (see below).

3.2 X-Ray Crystallography

For each complex single crystals of X-ray quality were obtained. The crystals of **L-Tb**, **L-Yb** and **L-Lu** each demonstrate a P_{31c} space group while that of **L-Gd** demonstrates a P_{-1} space group. The complexes all display the same coordination sphere whereby the metal ion resided in a monocapped octahedron coordination environment (Figure 1).[50] The lanthanide ion in each complex was seven-coordinate with the three imines and three oxygens of the salicylidene arms, as well as the tertiary bridging amine N4 involved in coordination. The complex possessed no coordinated solvent molecules due to protection of the coordination sphere by the bulky *t*-Bu groups in *ortho* position of the phenolates. For symmetry reasons the three Ln-O_{phenolate} (Ln-O1) are equivalent in **L-Tb**, **L-Yb** and **L-Lu**, similarly to the three Ln-N_{imine} (Ln-N1) bond distances. All the coordination bond distances were directly dependent on the lanthanide ion size. The Ln-O1 bond distances are 2.198, 2.153 and 2.148 Å for **L-Tb**, **L-Yb** and **L-Lu**, respectively, which followed the lanthanide contraction. The same applies for both the Ln-N1 bond distances at 2.716, 2.691 and 2.680 Å for **L-Tb**, **L-Yb** and **L-Lu**, respectively, and the Ln-N4 bond distances (2.479, 2.416 and 2.405 Å for **L-Tb**, **L-Yb** and **L-Lu**, respectively). For **L-Gd**, the coordination sphere is slightly dissymmetric. The Gd-O1, Gd-O2 and Gd-O3 bond distances are 2.216, 2.217 and 2.187 Å, respectively (mean value = 2.207 Å), while the Gd-N1, Gd-N2 and Gd-N3 bond distances (Gd-N_{imine}) are 2.505, 2.535 and 2.512 Å (mean value = 2.517 Å), respectively. They represent the largest values within the series due to the larger ionic radius of the Gd^{III} ion. Noteworthy, for all the complexes the Ln-O1 (and Ln-O2, Ln-O3 for **L-Gd**) bond lengths compare fairly well with those determined for **L^{OMe}-Ln**. [27] The Ln-N1 (and Ln-N2, Ln-N3 for **L-Gd**) bond lengths are slightly shorter in **L-Ln**, likely due to the lower electron density at the N1 atom.

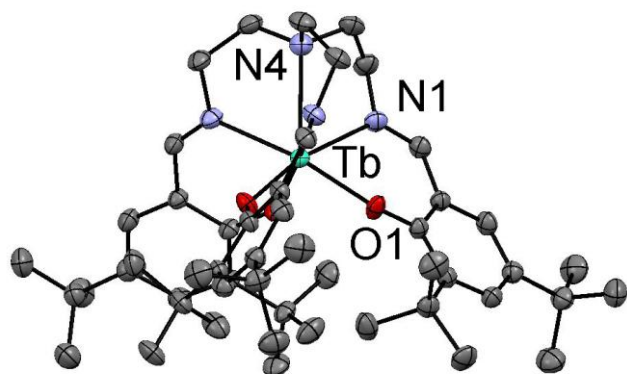


Figure 1. X-Ray crystal structure of **L-Tb** shown with 30 % thermal ellipsoids

Table 1. Coordination bond distances in **L-Ln** (in Å)

Complex	Ln-O _{phenolate}	Ln-N _{imine}	Ln-N _{amine}
L-Gd	2.216(2)	2.505(2)	2.792(2)
	2.217(2)	2.535(2)	
	2.187(3)	2.512(3)	
L-Tb	2.198(2) ^[a]	2.479(3) ^[a]	2.716(3)
L-Yb	2.153(2) ^[a]	2.416(3) ^[a]	2.691(3)
L-Lu	2.148(3) ^[a]	2.405(3) ^[a]	2.680(3)

^[a] The three salicylidene moieties are equivalent. Ln-O_{phenolate} and Ln-N_{imine} correspond to Ln-O1 and Ln-N1, respectively.

3.3 Electrochemistry

The easily detectable oxidation of the complexes is important for the determination of their potential as redox probes. For this reason the complexes were analysed via cyclic voltammetry (CV), rotating disk electrode (RDE) and differential potential voltammetry (DPV). Their electrochemical behavior was investigated in CH₃CN:CH₂Cl₂ (8:2) solution containing tetra-*n*-butylammonium perchlorate (TBAP) as supporting electrolyte. The CV curve of **L-Yb** (Figure 2), demonstrated three quasi-reversible oxidation events at $E^1_{1/2} = 0.37$ V, $E^2_{1/2} = 0.64$ V, $E^3_{1/2} = 0.85$ V vs. Fc⁺/Fc at 298 K, confirmed to be one-electron oxidations by RDE experiments and coulometry. Each of the complexes demonstrated similar redox behavior at 298 K. The three one-electron oxidations were assigned to the successive oxidation of the phenolate oxygens to the phenoxyl species. Not surprisingly, the oxidation waves are anodically shifted in comparison to **L^{OMe}-Ln** [27] due to the lower electron-donating ability of the *tert*-butyl groups. [37, 38] The first redox process depends only

marginally on the lanthanide ion, the $E_{1/2}^1$ values being similar within 0.02 V. The second and third redox processes are more dependent on the lanthanide ion, the smaller ions showing the higher oxidation potentials. This evolution likely arises from the shorter coordination bonds for smaller lanthanides, which bring the positive charge closer to the redox-active phenolate moieties. The $\Delta E_{1/2}^{1-2}$ was calculated according to $E_{1/2}^2 - E_{1/2}^1$. At room temperature it ranges between *ca.* 0.27 V for the shortest lanthanide ions (**L-Lu**, **L-Yb**) and 0.10 V for the biggest one (**L-Gd**), with an intermediate value for **L-Tb** (0.16 V). The range of $\Delta E_{1/2}^{1-2}$ is much larger than for the methoxy analogs (0.15-0.22 V for lanthanide varying from Nd^{III} to Lu^{III}), showing that the electrochemical communication is much more sensitive to the nature of the lanthanide in the present series. It is both strengthened for small lanthanides, whereas it is diminished for bigger metals in comparison to **L^{OMe}-Ln**. Interestingly, the same electrochemical characterization at 233 K show different CV curves. The current intensities decrease significantly, with minor shifts in potentials in the case of **L-Lu** and **L-Yb**, suggesting solubility issues at low temperature or passivation of the electrode. For the complexes with the largest lanthanide ions, namely **L-Tb** and **L-Gd**, no such decrease is observed. Instead, the oxidation potentials, especially $E_{1/2}^2$, are significantly cathodically shifted (Figure 2). In fact, these two complexes demonstrated a coalescing of the first two oxidation waves at 233 K. The temperature dependence of the potentials is depicted in ESI, while the potentials at 298 and 233 K are summarized in Table 2. We tentatively interpret this singular behaviour by considering an ECE mechanism, which involves an ion-pairing with the cations that is favoured for the largest lanthanides and at low temperatures. The association of the anion with the oxidized species would indeed contribute to a shielding of the charge, and consequently a decrease in $E_{1/2}^2$ and $E_{1/2}^3$. In an effort to confirm this hypothesis we additionally investigated the electrochemical behaviour of the complexes by using PF_6^- instead of ClO_4^- . As illustrated in Table 2, both **L-Gd** and **L-Yb** exhibit a temperature-dependence of the redox potentials that is similar to that observed in TBAP, but the potentials (especially $E_{1/2}^2$ and $E_{1/2}^3$) are effectively shifted in TBAPF_6 .

Table 2. Electrochemical data of **L-Ln** ^[a]

Complex	$E_{1/2}^1$	$E_{1/2}^2$	$E_{1/2}^3$
L-Gd (298 K)	0.39 ^[b]	0.49 ^[b]	0.69 ^[b]
L-Gd (233 K)	0.37 ^[b]	0.41 ^[b]	0.67 ^[b]
L-Tb (298 K)	0.39	0.54	0.73

L-Tb (233 K)	0.36 ^[c]		0.70
L-Yb (298 K)	0.37 ^[d]	0.64 ^[d]	0.81 ^[d]
L-Yb (233 K)	0.36 ^[d]	0.59 ^[d]	0.73 ^[d]
L-Lu (298 K)	0.36	0.63	0.76
L-Lu (233 K)	0.35	0.58	0.69sh

^[a] From DPV in CH₃CN:CH₂Cl₂ (8:2) solution containing 0.1 M TBAP. Determined at a vitreous carbon electrode by adding half of the pulse amplitude. The potentials are given in V and referenced to the redox Fc⁺/Fc redox couple (0.10 V ($\Delta E_p = 0.11$ V) vs. Ag/AgNO₃ 0.01 M).

^[b] The $E_{1/2}$ values in TBAPF₆ are 0.41, 0.51 and 0.71 V at high temperature and 0.36, 0.39 and 0.70 at low temperature.

^[c] The two successive monoelectronic processes could not be satisfactorily differentiated neither by DPV, not by CV.

^[d] The $E_{1/2}$ values in TBAPF₆ are 0.35, 0.58, 0.75 V at high temperature and 0.35, 0.61 and 0.77 at low temperature.

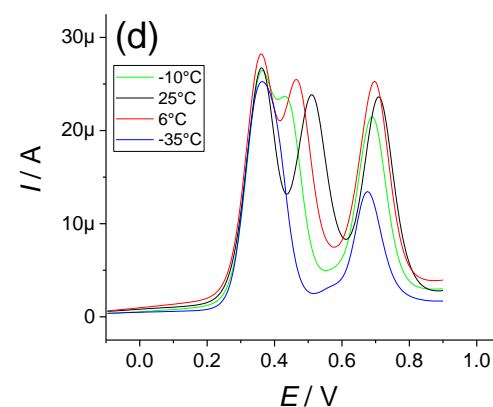
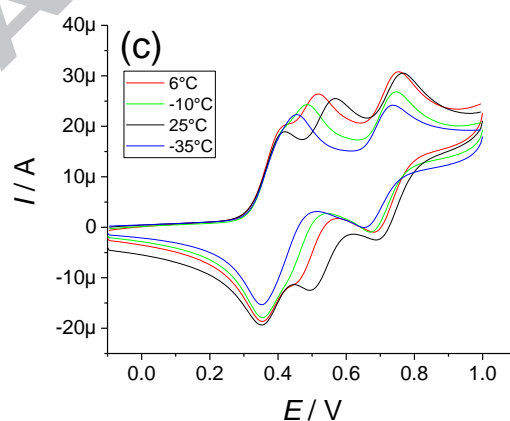
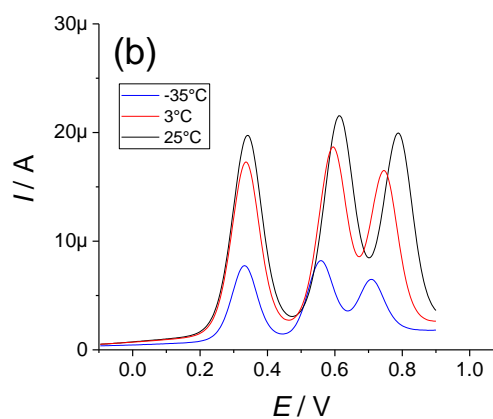
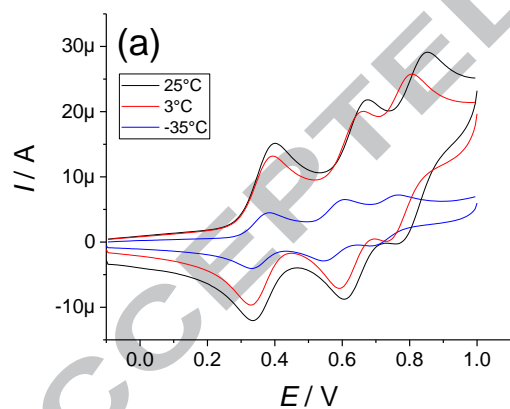


Figure 2. Electrochemical behavior of the lanthanide complexes **L-Ln** (0.5 mM) in CH₃CN : CH₂Cl₂ (8:2) containing 0.1 M TBAP examined by (a,c) cyclic voltammetry and (b,d) differential pulse voltammetry. (a,b) **L-Yb**; (c,d) **L-Gd**. Scan rate of the CV = 0.1 V / s; Pulse amplitude = 0.05 V. All the potentials are referenced to the Fc⁺/Fc redox couple.

3.3 UV-vis spectroscopy

The electronic spectrum of the complexes is dominated by an absorption band at around 370 nm. Both its high intensity ($\epsilon > 8000 \text{ M}^{-1} \text{ cm}^{-1}$) and position suggest that it corresponds to a π - π^* transition involving the salicylidene moieties.[51, 52] The addition of cerium ammonium nitrate (CAN), a strong one-electron oxidant, to the complexes resulted in a green colour change. It showed the gradual growth of a sharp and intense band at ca. 420 nm, reaching a plateau at 1 eq. whereby the one-electron oxidized species was formed.[53] An isosbestic is observed in every case at around 395 nm, confirming the clean conversion of **L-Ln** to **L-Ln⁺**. The new band in the 400-450 nm range is the hallmark of phenoxy radical species, supporting a ligand-centered oxidation of the complexes.[38] According to literature this band corresponds to the π - π^* transition of the phenoxy moieties [51, 52, 54-56] and it is blue-shifted in the **L-Ln⁺** radical complexes when compared to their methoxy derivatives.[38] Interestingly, the addition of over-stoichiometric amounts of CAN did not produce further growth of the phenoxy band, presumably due to fast decomposition of the over-oxidized radical species.[27] The consumption of Ce^{IV} above 1 eq. added is indeed confirmed by the decrease of the salicylidene band around 370 nm. In the case of **L-Gd** the addition of more than one molar equivalent of CAN even promotes decomposition of the radical species, as verified by the decrease in intensity of the band at 422 nm. These titrations show that the monooxidized species are accessible via CAN oxidation, which supports the hypothesis that the counter-ion and electrolyte play an important role in stabilizing the monoradical species against disproportionation. Such behaviour was previously reported in d-transition metal complexes.[57, 58] We will therefore focus our discussion only on the neutral and monocation in the next sections.

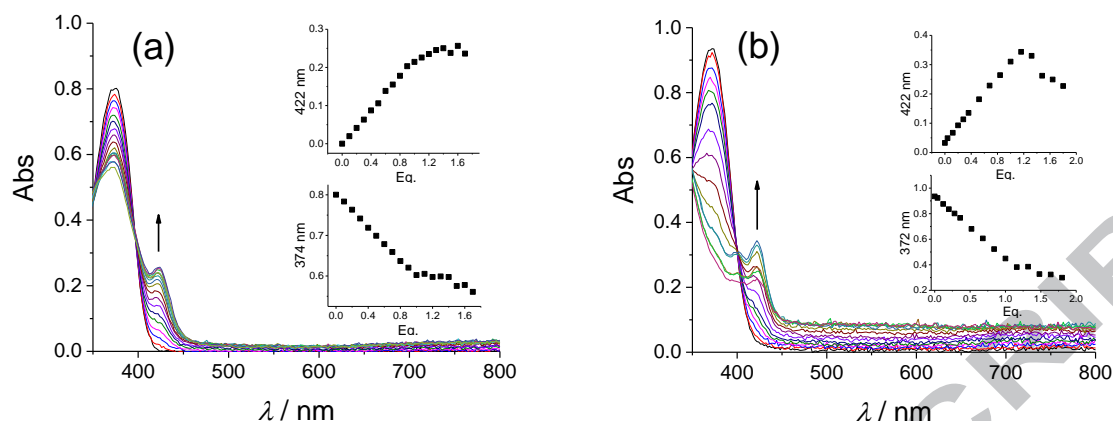


Figure 3. UV vis absorption spectra of the lanthanide complexes (a) **L-Lu** and (b) **L-Gd** (0.1 mM) in $\text{CH}_3\text{CN} : \text{CH}_2\text{Cl}_2$ (8:2) upon the addition of the one-electron oxidizing agent cerium ammonium nitrate (CAN). Inset: Absorption at given wavelengths upon addition of CAN. $T = 233 \text{ K}$; $l = 1.000 \text{ cm}$.

Table 3. UV-Vis data of **L-Ln**

Complex	λ [nm] (ϵ [$\text{M}^{-1}\cdot\text{cm}^{-1}$])	Complex	λ [nm] (ϵ [$\text{M}^{-1}\cdot\text{cm}^{-1}$])
L-Lu ^[a]	374 (8100)	L-Lu ⁺ ^[b]	422 (2600)
L-Yb ^[a]	376 (11000)	L-Yb ⁺ ^[b]	420 (4600)
L-Gd ^[a]	376 (9100)	L-Gd ⁺ ^[b]	422 (3100)
L-Tb ^[a]	376 (9200)	L-Tb ⁺ ^[b]	426 (4606)

^[a] In $\text{CH}_3\text{CN}:\text{CH}_2\text{Cl}_2$ (8:2) solution at 298 K.

^[b] Generated by addition of one eq. of cerium ammonium nitrate (CAN) at 233 K. In $\text{CH}_3\text{CN}:\text{CH}_2\text{Cl}_2$ (8:2) solution.

3.4 Electron Paramagnetic Resonance (EPR) spectroscopy

The spectrum of the cation **L-Lu**⁺ is the most straightforward to analyze due to the diamagnetism of the metal center. It consists of a single isotropic resonance at $g = 2.001$, with a peak-to-peak linewidth of 1.1 mT (Figure 4a). This signal is reminiscent of organic radicals, indicating that **L-Lu**⁺ is a Lu^{III} -phenoxy radical complex. The fact that the g_{iso} value is slightly lower than that typically observed for free phenoxy species (2.005) suggests that the radical is coordinated to the lanthanide ion in **L-Lu**⁺. The other complexes **L-Tb**, **L-Gd** and

L-Yb are paramagnetic species under their neutral forms, and could be characterized by EPR spectroscopy before oxidation.

The complex **L-Yb** shows resonances at $g = 3.9, 3.2$ and 2.8 (shoulder), which correspond to the parallel features of the Yb^{III} ion ($S = 1/2$). The main central line is associated to the even isotopes, while the peripheral ones are assigned to the odd isotopes $^{171}\text{Yb}^{\text{III}}$ and $^{173}\text{Yb}^{\text{III}}$. This spectrum (Figure 4b) resembles that measured for **L^{OMe}-Yb**, [27] with a small shift in g values due to the slightly different electronics of the ligand. As for the methoxy analog the line broadening does not allow for the observation of the Tb hyperfine splitting in the case of the odd isotopes. The one-electron oxidation of **L-Yb** into **L-Yb⁺** results in a total quenching of the lanthanide-associated resonances (Figure 4b). A sharp line of very low intensity can be detected at around $g = 2$, which is assigned to a minor ($S = 1/2$) radical decomposition product. These results indicate that **L-Yb⁺** is either hard to detect at the X-Band frequency, or EPR-silent due to magnetic interactions between the radical and the metal spins.

The complex **L-Gd** displays a set of resonances that easily saturate at the g_{eff} values of $1.6, 2$ and 2.5 , as expected for S-state ($4f^7$) metal ions. As for the ytterbium complex the overall shape of the spectrum roughly matches that of the methoxy analog, with a slight shift of the g values. Given the absence of crystal structure for **L^{OMe}-Gd**, [27] the present data therefore supports a similar environment of the metal center. Additional resonances of much lower intensity are observed in the low field region (Figure 4c), as expected for this ($S = 7/2$) spin system. The oxidation is demonstrated by a quenching of the main resonances, with shifts in the low field region. Both suggest that a magnetic coupling is operating between the ligand radical and the metal center, as for **L-Yb⁺**. The spectrum recorded in parallel polarization shows a multi-line pattern in the 0-600 mT region, which confirms the formation of an integer spin system upon oxidation, and therefore the removal of a single electron. The lack of additional HF-EPR and magnetic data (due to the instability of the radical) precludes going further in the analysis of this complicated spectrum. [59]

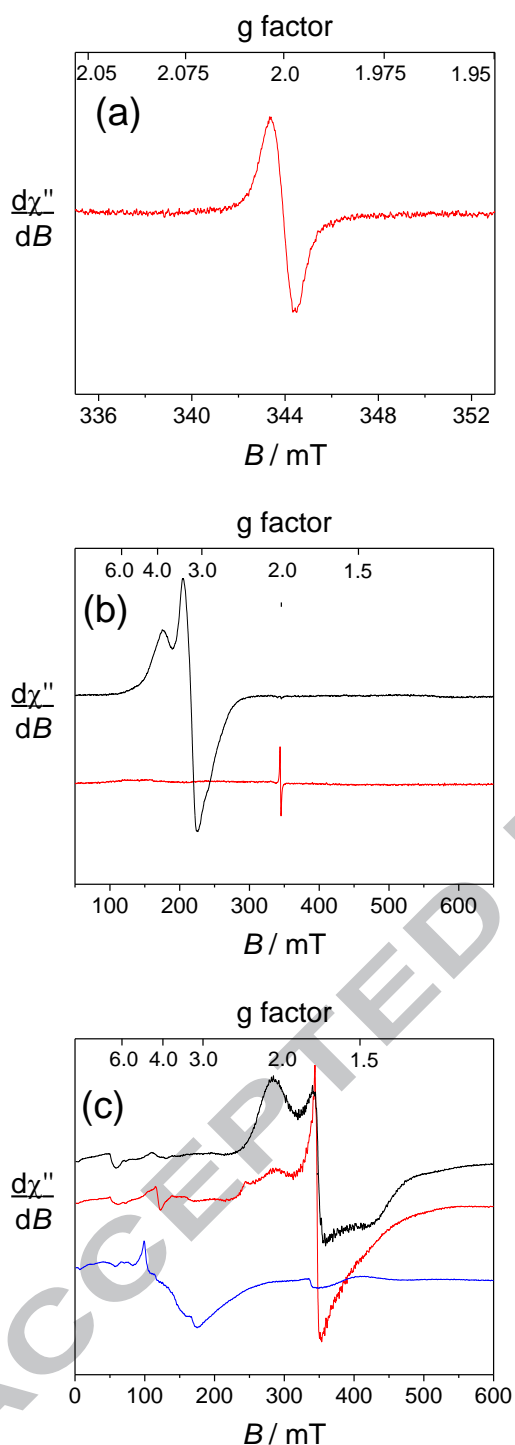


Figure 4. X-Band EPR spectra of 0.5 mM solutions of the lanthanide complexes in frozen $\text{CH}_2\text{Cl}_2:\text{CH}_3\text{CN}$ (2:8) before (black) and after (red) oxidation. The blue line is the spectrum in parallel mode, the other are recorded in perpendicular mode. (a) **L-Lu**, (b) **L-Yb**, (c) **L-Gd**. Microwave Freq. 9.63 GHz (9.36 GHz in parallel mode); Mod. Freq. 100 KHz; Mod. Amp. (a) 0.2 mT, (b-c) 0.4 mT (or 0.7 mT in parallel mode); Microwave power, (a,c) 2 mW or (b and c in parallel mode) 20 mW. $T = 7$ K.

The EPR spectrum **L-Tb** was proved to be difficult to observe. At 7 K it shows a very broad anisotropic signal at around $g = 3.2$, whose resolution could not be improved by adding supporting electrolyte. The main resonance resembles that reported for the Tb^{III} complex of the 3-hydroxypicolinamide,[60] but cannot be further interpreted owing to the poor resolution and exceedingly large linewidth. The spectrum of the one-electron oxidized **L-Tb**⁺ was strikingly different, but remains of low intensity. It shows two components. The first one is a sharp isotropic line of low intensity at $g = 2.00$, i.e. in a region where the phenoxyl resonance is expected to be found. The second signal appears at fields lower than 100 mT, where the Tb^{III} resonances are expected to be found. This latter assignment is further supported by the observation of the Tb^{III} hyperfine splitting at $A_{\text{Tb}} = 27$ mT and the enhancement of the signal under parallel polarization. The simultaneous presence of both signals suggests that either the terbium is surprisingly uncoupled to the radical in the cation, or that **L-Tb**⁺ is difficult to detect and that the present spectrum is the sum of two decomposition products (Tb^{III} complex and free radical). We investigated the response to power of the spectra and observed that the signal at $g = 2.00$ saturates much more easily than the Tb^{III} signal, which argues for the second hypothesis.

Altogether these EPR data support phenoxyl radical generation upon oxidation, and demonstrate that the radical remains close to the metal center whatever the lanthanide.

3.5 DFT calculations

The electronic structure of the lutetium complex has been investigated by theoretical calculations. We used a full-electron approach that includes relativistic effects through the ZORA Hamiltonian. The computational cost of this methodology makes that this investigation is restricted to the lowest spin systems, e.g. the lutetium and ytterbium complexes. Full geometry optimization shows that neutral **L-Lu** exhibits a C_{3v} symmetry, in agreement with the X-Ray diffraction and solution NMR data. The Lu-O1 and Lu-N1 bond distances are reasonably well predicted, with calculated values of 2.163 and 2.451 Å, respectively, vs. 2.148 and 2.405 Å, experimentally. Similarly, the optimized **L-Yb** shows a symmetrical coordination sphere with longer Ln-O1 and Ln-N1 bonds (2.176 and 2.463 Å, respectively), due to the largest ionic radius of the metal ion. The Lu-N4 bond is much weaker, which explains the larger deviation from experiment (2.901 and 2.895 Å for **L-Lu** and **L-Yb**, respectively). Such behavior was already reported for the methoxy derivatives.[27] The geometry optimized cations **L-Lu**⁺ and **L-Yb**⁺ both show a C_{3v} symmetry, similarly to the neutral precursors. In other terms, oxidation is not preferentially localized on one

phenolate ring, in contrast to the methoxy derivatives. This trend is in line with that reported for one-electron oxidized Ni^{II} salen complexes, which are symmetrical (full delocalization of the SOMO) with a *tert*-butyl para substituent[30, 34, 37] but dissymmetrical (localized phenoxy) with a methoxy para substituent.[32, 34, 37] Detailed examination of the metrical parameters shows that the Ln-O1 bonds undergo an elongation of ca. 0.02 Å upon oxidation (2.185 and 2.197-2.200 Å for **L-Lu**⁺ and **L-Yb**⁺, respectively), indicative of a weaker donating ability of the phenoxy ring in comparison to a phenolate. Conversely, the Ln-N1 bond shortens by 0.02 Å (2.434 and 2.445 Å for **L-Lu**⁺ and **L-Yb**⁺, respectively) and the Ln-N4 one by 0.10 Å (2.807 and 2.800 Å for **L-Lu**⁺ and **L-Yb**⁺, respectively). A slight but sizeable quinoidal redistribution of bond distances is observed in each peripheral ring, with a shortening of the C1-O1 bond by 0.01 Å. It is less than expected for the formation of a phenoxy radical due to delocalization of the radical SOMO over the three arms of the ligand. The Mulliken spin population on selected atoms is listed in Table 4 and compared to that calculated at the same level of theory for the methoxy derivatives.[27] The data show that apart from full delocalization over the three arms, the methoxy to *tert*-butyl substitution induces spin redistribution in each ring, with increased spin population at the C2, C4 and C6 atoms, at the expense of the C1 atom and the para (methoxy) substituent. It also shows that the nature of the lanthanide does not influence significantly the spin population on the ligand.

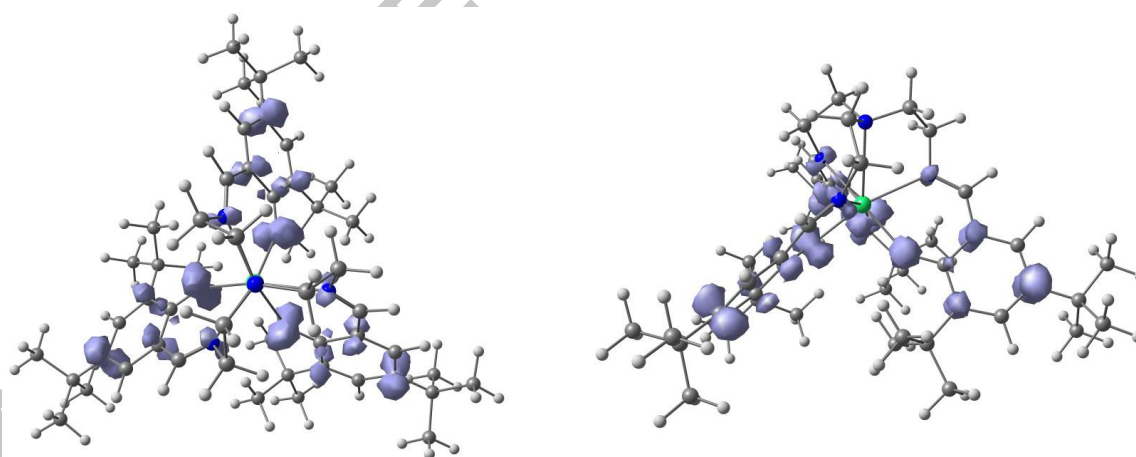
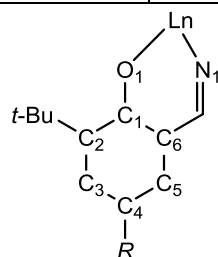


Figure 5. Top and side views of the spin density plot of **L-Lu**⁺ (B3LYP/TZVP/SARC(Lu)/ZORA)

Table 4. Mulliken spin population on selected atoms in the complexes **L-Ln**⁺ [a]

Ln	R	O1	C1	C2	C4	C6
Lu	<i>t</i> -Bu ^[b]	0.09	0.03	0.06	0.11	0.06
Lu	OMe ^[c]	0.12	0.06	0.06	0.10	0.04
		0.07	0.04	0.04	0.06	0.02

		0.06 Mean: 0.083	0.04 Mean: 0.047	0.03 Mean: 0.043	0.05 Mean: 0.07	0.02 Mean: 0.027
Yb	<i>t</i> -Bu ^[b]	0.09	0.03	0.06	0.11	0.06
Yb	OMe ^[c]	0.13 0.08 0.07 Mean: 0.093	0.06 0.04 0.04 Mean: 0.047	0.07 0.04 0.04 Mean: 0.05	0.10 0.06 0.06 Mean: 0.073	0.04 0.02 0.02 Mean: 0.027



[a] From a B3LYP/TZVP/SARC(Lu)/ZORA calculation. The atom numbering is indicated above.

[b] The three phenol-based units are equivalent.

[c] From ref. The three phenol-based units are inequivalent.

3.6 Luminescence

The lanthanide ions in particular have been chosen for their exceptional photophysical properties. The optical properties of the complexes **L-Ln** (Ln = Tb^{III}, Nd^{III}, Yb^{III}, Gd^{III}) are shown in Figure 6 at 298 K and 233 K. At room temperature the emission spectrum of **L-Gd** under excitation in the $\pi \rightarrow \pi^*$ and $n \rightarrow \pi^*$ absorption band revealed in the UV-vis spectrum results in a ligand-centred emission as one intense and broad band at 440 nm whose intensity quickly diminishes when a short delay (0.05 μ s) is enforced and therefore has been attributed to the $^1\pi\pi^*$ ligand state. At low temperature this band can no longer be detected but another band at 530 nm appears with a single-exponential time decay of 1.87(5) ms and is therefore assigned to the $^3\pi\pi^*$ state. The **L-Lu** complex confirmed the position of the triplet energy level with a lifetime of 19.1(1) ms. For the emissive **L-Tb** and **L-Tb** complexes, the two $^1\pi\pi^*$ and $^3\pi\pi^*$ ligand levels were quenched due to population of the lowest lying lanthanide energy level. At 298 K the visible Tb emission of **L-Tb** cannot be observed due to quenching by the low-lying $^3\pi\pi^*$ state triplet state with respect to the Tb(5D_4) excited state. However, at low temperature (77 K), the emission spectrum displays $^5D_4 \rightarrow ^7F_J$ for J = 6-0 and is dominated by the transition to 7F_5 . This is indicative of sensitization *via* a ligand-to-metal energy transfer and as a result of the energy of the 0-phonon transition we thus conclude the Tb(5D_4) excited emission is most efficiently sensitized by the singlet state, as previously observed in Tb^{III} complexes with Schiff-base ligands.[61, 62]

Since the ligand possesses a low-energy triplet, it appears that it would be suited for sensitization of Yb^{III} . The emission spectrum of the corresponding complex **L-Yb** consists of an intense set of emission lines assigned to the ${}^2\text{F}_{5/2} \rightarrow {}^2\text{F}_{7/2}$ transition with a total quenching of the ligand emissive states, which was dominated by narrow line like emission bands with four main crystal field components in the range 960-1200 nm. Measurements at different temperatures show that the overall shape of the Yb^{III} spectrum remains the same, except for a slight broadening and a more intense peak appearing at 940 nm from a thermally populated ${}^2\text{F}_{5/2}$ state. The excitation spectrum of the complex **L-Yb** clearly demonstrated the antenna effect of the ligand. The population of the excited states of the metal via the ligand is demonstrated by the excitation spectra which display two components between 320 and 395 nm (Figure 7), matching perfectly the low-energy absorption band of the UV spectra (Figure 4).

The emission of the Tb^{III} and Yb^{III} complexes permitted the detection of distinct changes between the neutral and oxidised phenoxyl complexes. The formation of the one-electron oxidised product **L-Ln⁺** can be evidenced by a strong quenching of the metal-centred luminescence. Figure 7 illustrates the change in the luminescence upon addition of the chemical oxidant CAN to $\text{CH}_3\text{CN} : \text{CH}_2\text{Cl}_2$ (8:2) solutions of the **L-Ln** (Tb, Yb). A very substantial decrease in the luminescence signal was observed. The extent of quenching observed was 83 and 93 % respectively for the **L-Tb⁺** and **L-Yb⁺**. This very intense intramolecular quenching indicates that the lanthanides complexes **L-Ln** are extremely sensitive to the oxidation state of the ligand. Noteworthy, the quenching is slightly more efficient than for the **L^{OMe}-Yb** complex (83 %), while for **L^{OMe}-Tb** no emission was observed neither before or after oxidation. This shows that these complexes could be very promising as redox-sensitive luminescent probes both in the visible and NIR regions.

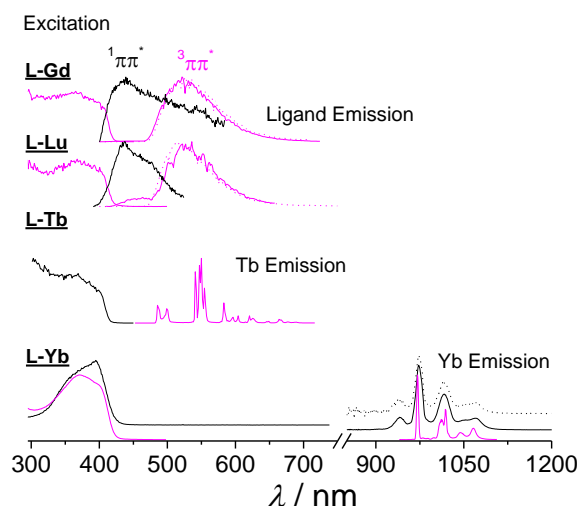


Figure 6. Normalized emission ($\lambda_{\text{ex}} = 375$ nm) and excitation spectra ($\lambda_{\text{an}} = 520, 520, 550$ and 976 nm for Gd, Lu, Tb and Yb, respectively) of **L-Ln** (Ln = Gd, Lu, Tb and Yb). The spectra were recorded at 0.5 mM in acetonitrile. $T = 77$ K (pink lines), 298 K (black lines).

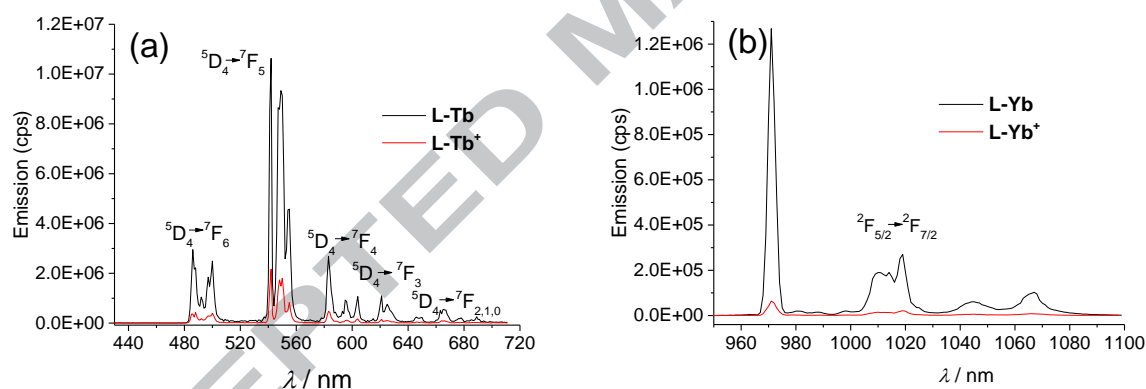


Figure 7. Emission spectra ($\lambda_{\text{ex}} = 375$ nm) of (a) **L-Tb** and (b) **L-Yb** before (black lines) and after (red lines) oxidation with CAN (1 eq.) at 0.5 mM in acetonitrile at 77 K.

4. Conclusion

We reported a series of four complexes **L-Ln**, (Ln = Gd^{III} , Tb^{III} , Yb^{III} , Lu^{III}), wherein the metal resides in a monocapped octahedron environment. They all demonstrated a 3-electron oxidation behavior. As expected from the lower electron donating ability of the *tert*-butyl substituent the potentials are higher than for the methoxy analogs. The potential of the 1st oxidation event does not differ significantly in the series, in contrast to the 2nd and 3rd redox processes. They follow the lanthanide contraction and exhibit a unique temperature-dependent behavior for the largest lanthanides. We establish that the smaller the cation, the higher the

oxidation potential and the larger the separation between the 1st and 2nd oxidation waves. The presence of the characteristic $\pi-\pi^*$ transition at 420 nm in the UV-Vis spectrum of the cations confirms that the oxidation products are phenoxyl radical species. This assignment is corroborated by EPR spectroscopy, which shows a resonance at $g = 2.001$ for **L-Lu⁺**. The other cations show mostly a quenching of the EPR signal, supporting a magnetic coupling between the phenoxyl moiety and the metal ion. For both **L-Lu⁺** and **LYb⁺** DFT calculations predict the radical to be delocalized over the three arms. Finally, **L-Tb** and **L-Yb** are luminescent, but demonstrated a dramatic quenching of the luminescence of the lanthanide upon oxidation. This proves redox active probes with a luminescent response.

Acknowledgements

The authors sincerely thank the Labex ARCANE (ANR-11-LABX-0003-01) and the French National Agency for Research (Co-Lhanta/ANR-13-BS08-0011-01) for financial support, as well as the CECIC cluster, which provided the computational facilities.

References

- [1] F. Hyodo, B.P. Soule, K.-i. Matsumoto, S. Matusmoto, J.A. Cook, E. Hyodo, A.L. Sowers, M.C. Krishna, J.B. Mitchell, Assessment of tissue redox status using metabolic responsive contrast agents and magnetic resonance imaging, *J. Pharm. Pharmacol.*, 60 (2008) 1049-1060.
- [2] A.J. Meyer, T.P. Dick, Fluorescent protein-based redox probes, *Antiox. Redox Signal.*, 13 (2010) 621-650.
- [3] A.L. Harris, Hypoxia — a key regulatory factor in tumour growth, *Nat. Rev. Cancer*, 2 (2002) 38.
- [4] J.T. Erler, K.L. Bennewith, M. Nicolau, N. Dornhöfer, C. Kong, Q.-T. Le, J.-T.A. Chi, S.S. Jeffrey, A.J. Giaccia, Lysyl oxidase is essential for hypoxia-induced metastasis, *Nature*, 440 (2006) 1222.
- [5] D.M. Gilkes, G.L. Semenza, D. Wirtz, Hypoxia and the extracellular matrix: drivers of tumour metastasis, *Nat. Rev. Cancer*, 14 (2014) 430.
- [6] N. McCarthy, Micro changes, *Nat. Rev. Cancer*, 14 (2014) 382.
- [7] B. Thienpont, J. Steinbacher, H. Zhao, F. D'Anna, A. Kuchnio, A. Ploumakis, B. Ghesquière, L. Van Dyck, B. Boeckx, L. Schoonjans, E. Hermans, F. Amant, V.N. Kristensen, K.P. Koh, M. Mazzone, M.L. Coleman, T. Carell, P. Carmeliet, D. Lambrechts, Tumour hypoxia causes DNA hypermethylation by reducing TET activity, *Nature*, 537 (2016) 63.
- [8] H. Abe, H. Semba, N. Takeda, The Roles of Hypoxia Signaling in the Pathogenesis of Cardiovascular Diseases, *J. Atheroscler. Thromb.*, 24 (2017) 884-894.
- [9] F. Zhang, R. Zhong, H. Qi, S. Li, C. Cheng, X. Liu, Y. Liu, W. Le, Impacts of Acute Hypoxia on Alzheimer's Disease-Like Pathologies in APP^{sw}/PS1^{dE9} Mice and Their Wild Type Littermates, *Front. Neurosc.*, 12 (2018).

- [10] S. Matsumoto, H. Yasui, J.B. Mitchell, M.C. Krishna, Imaging Cycling Tumor Hypoxia, *Cancer Res.*, 70 (2010) 10019-10023.
- [11] F.C. Gaertner, M. Souvatzoglou, G. Brix, A.J. Beer, Imaging of Hypoxia Using PET and MRI, *Curr. Pharm. Biotech.*, 13 (2012) 552-570.
- [12] D. Yang, H.Y. Tian, T.N. Zang, M. Li, Y. Zhou, J.F. Zhang, Hypoxia imaging in cells and tumor tissues using a highly selective fluorescent nitroreductase probe, *Sci. Rep.*, 7 (2017) 9174.
- [13] Z. Zhelev, V. Gadjeva, I. Aoki, R. Bakalova, T. Saga, Cell-penetrating nitroxides as molecular sensors for imaging of cancer in vivo, based on tissue redox activity, *Mol. Biosyst.*, 8 (2012) 2733-2740.
- [14] J.-C.G. Bünzli, C. Piguet, Taking advantage of luminescent lanthanide ions, *Chem. Soc. Rev.*, 34 (2005) 1048-1077.
- [15] J.-C.G. Bünzli, Benefiting from the unique properties of lanthanide ions, *Acc. Chem. Res.*, 39 (2006) 53-61.
- [16] A. de Bettencourt-Dias, Introduction to lanthanide ion luminescence, *Luminescence of Lanthanide Ions in Coordination Compounds and Nanomaterials*, (2014) 1-48.
- [17] B. Song, G. Wang, M. Tan, J. Yuan, A Europium(III) Complex as an Efficient Singlet Oxygen Luminescence Probe, *J. Am. Chem. Soc.*, 128 (2006) 13442-13450.
- [18] S. Cuihong, Y. Zhiqiang, W. Guilan, Y. Jingli, G. Yafeng, A Lanthanide-Complex-Based Ratiometric Luminescent Probe Specific for Peroxynitrite, *Chem. – Eur. J.*, 16 (2010) 6464-6472.
- [19] A.R. Lippert, T. Gschneidtner, C.J. Chang, Lanthanide-based luminescent probes for selective time-gated detection of hydrogen peroxide in water and in living cells, *Chem. Commun.*, 46 (2010) 7510-7512.
- [20] J. Hong, Y. Zhuang, X. Ji, X. Guo, A long-lived luminescence and EPR bimodal lanthanide-based probe for free radicals, *Analyst*, 136 (2011) 2464-2470.
- [21] X. Ji, J. Hong, X. Guo, Ultrasensitive detection of phenolic compounds based on a spin-labeled luminescent lanthanide complex, *Analyst*, 137 (2012) 710-715.
- [22] Y. Xiao, Z. Ye, G. Wang, J. Yuan, A Ratiometric Luminescence Probe for Highly Reactive Oxygen Species Based on Lanthanide Complexes, *Inorg. Chem.*, 51 (2012) 2940-2946.
- [23] S. Csongor, P. Elias, I.N. O., B.K. Eszter, A Versatile Long-Wavelength-Absorbing Scaffold for Eu-Based Responsive Probes, *Chem. – Eur. J.*, 19 (2013) 3099-3109.
- [24] K.L. Peterson, M.J. Margherio, P. Doan, K.T. Wilke, V.C. Pierre, Basis for Sensitive and Selective Time-Delayed Luminescence Detection of Hydroxyl Radical by Lanthanide Complexes, *Inorg. Chem.*, 52 (2013) 9390-9398.
- [25] J.K. Molloy, O. Jarjays, C. Philouze, L. Fedele, D. Imbert, F. Thomas, A redox active switch for lanthanide luminescence in phenolate complexes, *Chem. Commun.*, 53 (2017) 605-608.
- [26] J. Wu, Y. Yang, L. Zhang, H. Wang, M. Yang, J. Yuan, A visible-light-excited Eu³⁺ complex-based luminescent probe for highly sensitive time-gated luminescence imaging detection of intracellular peroxynitrite, *J. Mat. Chem. B*, 5 (2017) 2322-2329.
- [27] J.K. Molloy, C. Philouze, L. Fedele, D. Imbert, O. Jarjays, F. Thomas, Seven-coordinate lanthanide complexes with a tripodal redox active ligand: structural, electrochemical and spectroscopic investigations, *Dalton Trans.*, (2018).
- [28] J. Molloy, K., O. Jarjays, C. Philouze, L. Fedele, D. Imbert, F. Thomas, A redox active switch for lanthanide luminescence in phenolate complexes, *Chem. Commun.*, 53 (2017) 605-608.

- [29] O. Rotthaus, O. Jarjayes, C. Perez Del Valle, C. Philouze, F. Thomas, A versatile electronic hole in one-electron oxidized Ni(II) bis-salicylidene phenylenediamine complexes, *Chem. Commun.*, (2007) 4462-4464.
- [30] T. Storr, E.C. Wasinger, R.C. Pratt, T.D.P. Stack, The Geometric and Electronic Structure of a One-Electron-Oxidized Nickel(II) Bis(salicylidene)diamine Complex, *Angew. Chem. Int. Ed.*, 46 (2007) 5198-5201.
- [31] A. Kochem, M. Orio, O. Jarjayes, F. Neese, F. Thomas, Unsymmetrical one-electron oxidized Ni(ii)-bis(salicylidene) complexes: a protonation-induced shift of the oxidation site, *Chem. Commun.*, 46 (2010) 6765-6767.
- [32] M. Orio, O. Jarjayes, H. Kanso, C. Philouze, F. Neese, F. Thomas, X-Ray Structures of Copper(II) and Nickel(II) Radical Salen Complexes: The Preference of Galactose Oxidase for Copper(II), *Angew. Chem. Int. Ed.*, 49 (2010) 4989-4992.
- [33] P. Verma, R.C. Pratt, T. Storr, E.C. Wasinger, T.D.P. Stack, Sulfanyl stabilization of copper-bonded phenoxy radicals in model complexes and galactose oxidase, *Proc. Natl. Acad. Sci. U.S.A.*, 108 (2011) 18600-18605.
- [34] L. Chiang, A. Kochem, O. Jarjayes, T.J. Dunn, H. Vezin, M. Sakaguchi, T. Ogura, M. Orio, Y. Shimazaki, F. Thomas, T. Storr, Radical Localization in a Series of Symmetric Ni(II) Complexes with Oxidized Salen Ligands, *Chem. – Eur. J.*, 18 (2012) 14117-14127.
- [35] R.C. Pratt, C.T. Lyons, E.C. Wasinger, T.D.P. Stack, Electrochemical and Spectroscopic Effects of Mixed Substituents in Bis(phenolate)–Copper(II) Galactose Oxidase Model Complexes, *J. Am. Chem. Soc.*, 134 (2012) 7367-7377.
- [36] C.T. Lyons, T.D.P. Stack, Recent Advances in Phenoxy Radical Complexes of Salen-type Ligands as Mixed-valent Galactose Oxidase Models, *Coord. Chem. Rev.*, 257 (2013) 528-540.
- [37] F. Thomas, Ligand-centred Oxidative Chemistry in Sterically Hindered Salen Complexes: an Interesting case with Nickel, *Dalton Trans.*, 45 (2016) 10866.
- [38] F. Thomas, Coordinated Phenoxy Radicals, in: R.G. Hicks (Ed.) *Stable Radicals: Fundamentals and Applied Aspects of Odd-Electron Compounds*, John Wiley and Sons, Chichester, 2010, pp. 281-316.
- [39] M.W. Essig, D. Webster Keogh, B.L. Scott, J.G. Watkin, Synthesis and structural characterization of the lanthanide Schiff-base complexes $\{N[CH_2CH_2N(CH_2O-3,5-t-Bu_2C_6H_2)]_3\}Ln$ (Ln=Sm, Nd), *Polyhedron*, 20 (2001) 373-377.
- [40] D. Lionetti, V.W. Day, J.D. Blakemore, Noncovalent immobilization and surface characterization of lanthanide complexes on carbon electrodes, *Dalton Trans.*, 46 (2017) 11779-11789.
- [41] O.V. Dolomanov, L.J. Bourhis, R.J. Gildea, J.A.K. Howard, H. Puschmann, Olex2: A Complete Structure Solution, Refinement and Analysis Program, *J. Appl. Cryst.*, 42 (2009) 339-340.
- [42] F. Neese, The ORCA Program System, *WIREs Comput. Mol. Sci.*, 2 (2012) 73-78.
- [43] A.D. Becke, Density-functional exchange-energy approximation with correct asymptotic behavior, *Phys. Rev. A*, 38 (1988) 3098-3100.
- [44] C. Lee, W. Yang, R.G. Parr, Development of the Colle-Salvetti Correlation-energy Formula into a Functional of the Electron Density, *Phys. Rev. B: Condens. Matter Mater. Phys.*, 37 (1988) 785-789.
- [45] C.v. Wüllen, Molecular density functional calculations in the regular relativistic approximation: Method, application to coinage metal diatomics, hydrides, fluorides and chlorides, and comparison with first-order relativistic calculations, *J. Chem. Phys.*, 109 (1998) 392-399.

- [46] F. Neese, F. Wennmohs, A. Hansen, U. Becker, Efficient, approximate and parallel Hartree–Fock and hybrid DFT calculations. A ‘chain-of-spheres’ algorithm for the Hartree–Fock exchange, *Chem. Phys.*, 356 (2009) 98-109.
- [47] D.A. Pantazis, F. Neese, All-Electron Scalar Relativistic Basis Sets for the Lanthanides, *J. Chem. Theory Comput.*, 5 (2009) 2229-2238.
- [48] D.A. Pantazis, X.-Y. Chen, C.R. Landis, F. Neese, All-Electron Scalar Relativistic Basis Sets for Third-Row Transition Metal Atoms., *J. Chem. Theory Comput.*, 4 (2008) 908-919.
- [49] J. J. Parr, A. T. Ross, A.M.Z. Slawin, Complexes of Indium (III) with Tripodal Schiff Base Ligands, *Main Group Chem.*, 2 (1997) 243-249.
- [50] X.M. Hu, L.W. Xue, G.Q. Zhao, W.C. Yang, Synthesis, structures, and biological activity of terbium(III) and cobalt(III) complexes derived from tripodal Schiff bases, *Russ. J. Coord. Chem.*, 41 (2015) 197-201.
- [51] F. Thomas, O. Jarjayes, C. Duboc, C. Philouze, E. Saint-Aman, J.-L. Pierre, Intramolecularly Hydrogen-bonded versus Copper(II) Coordinated Mono- and Bis-phenoxy Radicals, *Dalton Trans.*, (2004) 2662-2669.
- [52] O. Rotthaus, O. Jarjayes, F. Thomas, C. Philouze, E. Saint-Aman, J.-L. Pierre, Up to four phenoxy radicals coordinated to two metal ions in copper and zinc complexes?, *Dalton Trans.*, (2007) 889-895.
- [53] The kinetics of the CAN oxidation was proved to be complete with the msec time scale at room temperature, as revealed by stopped-flow measurements. These stopped-flow measurements also show that the oxidized species decayed extremely fast, with the decay finished after 40 ms at room temperature.
- [54] A. Philibert, F. Thomas, C. Philouze, S. Hamman, E. Saint-Aman, F.-L. Pierre, Galactose Oxidase Models: Tuning the Properties of CuII Phenoxy Radicals, *Chem. – Eur. J.*, 9 (2003) 3803-3812.
- [55] F. Michel, F. Thomas, S. Hamman, E. Saint-Aman, C. Bucher, J.-L. Pierre, Galactose Oxidase Models: Solution Chemistry, and Phenoxy Radical Generation Mediated by the Copper Status, *Chem. – Eur. J.*, 10 (2004) 4115-4125.
- [56] F. Michel, F. Thomas, S. Hamman, C. Philouze, E. Saint-Aman, J.-L. Pierre, Galactose Oxidase Models: Creation and Modification of Proton Transfer Coupled to Copper(II) Coordination Processes in Pro-Phenoxy Ligands, *Eur. J. Inorg. Chem.*, 2006 (2006) 3684-3696.
- [57] D. Herebian, E. Bothe, F. Neese, T. Weyhermüller, K. Wieghardt, Molecular and Electronic Structures of Bis-(*o*-diiminobenzosemiquinonato)metal(II) Complexes (Ni, Pd, Pt), Their Monocations and -Anions, and of Dimeric Dications Containing Weak Metal–Metal Bonds, *J. Am. Chem. Soc.*, 125 (2003) 9116-9128.
- [58] N. Leconte, J. Moutet, T. Constantin, F. Molton, C. Philouze, F. Thomas, Coordination Chemistry of the Redox Non-Innocent Ligand Bis(2-amino-3,5-di-*tert*-butylphenyl)amine with Group 10 Metal Ions (Ni, Pd, Pt), *Eur. J. Inorg. Chem.*, (2018) 1752-1761.
- [59] A. Dei, D. Gatteschi, C.A. Massa, L.A. Pardi, S. Poussereau, L. Sorace, Spontaneous Symmetry Breaking in the Formation of a Dinuclear Gadolinium Semiquinonato Complex: Synthesis, High-Field EPR Studies, and Magnetic Properties, *Chem. – Eur. J.*, 6 (2000) 4580-4586.
- [60] T.P. Devi, P. Pengkiliya, L. Rajkumari, Interaction of 3-Hydroxypicolinamide with TbIII and its sensitizing effect on terbium luminescence as a function of pH and medium, *S. Afr. J. Chem.* 67 Durban Jan. 2014, 67 (2014) 218–225.
- [61] P. Guerriero, P.A. Vigato, J.-C.G. Bünzli, E. Moret, Macrocyclic complexes with lanthanoid salts part 38. Synthesis and luminescence study of homo- and hetero-binuclear complexes of lanthanides with a new cyclic compartmental Schiff base, *J. Chem. Soc., Dalton Trans.*, (1990) 647-655.

[62] R.C. Howell, K.V.N. Spence, I.A. Kahwa, A.J.P. White, D.J. Williams, The preparation and crystal and molecular structures of new luminescent Schiff-base complexes featuring coupled lanthanide(III) cations, *J. Chem. Soc., Dalton Trans.*, (1996) 961-968.

Highlights

- Tris(phenolato) lanthanide complexes (Gd, Tb, Yb, Lu) were crystallized.
- Oxidation affords phenoxy radical species.
- The tris(phenolato) terbium and ytterbium complexes are luminescent
- The luminescence is quenched upon oxidation

